1-1-2016

Magnetospheric Multiscale Observations Of Large-Amplitude, Parallel, Electrostatic Waves Associated With Magnetic Reconnection At The Magnetopause

S. Eriksson

D. M. Malaspina

A. Retino

P. A. Cassak

AGU PUBLICATIONS

Geophysical Research Letters

RESEARCH LETTER
10.1002/2016GL068992

Special Section:
First results from NASA's Magnetospheric Multiscale (MMS) Mission

Magnetospheric Multiscale observations of large-amplitude, parallel, electrostatic waves associated with magnetic reconnection at the magnetopause

R. E. Ergun[1,2], J. C. Holmes[1,2], K. A. Goodrich[1,2], F. D. Wilder[2], J. E Stawarz[1,2], S. Eriksson[2], D. L. Newman[3], S. J. Schwartz[2,4], M. V. Goldman[3], A. P. Sturner[1,2], D. M. Malaspina[2], M. E. Usanova[2], R. B. Torbert[5,6], M. Argall[5], P.-A. Lindqvist[7], Y. Khotyaintsev[8], J. L. Burch[6], R. J. Strangeway[9], C. T. Russell[9], C. J. Pollock[10], B. L. Giles[10], J. J. C. Dorelli[10], L. Avanov[10], M. Hesse[10], L. J. Chen[11], B. Lavraud[12,13], O. Le Contel[14], A. Retino[14], T. D. Phan[15], J. P. Eastwood[4], M. Oieroset[15], J. Drake[11], M. A. Shay[16], P. A. Cassak[17], R. Nakamura[18], M. Zhou[19], M. Ashour-Abdalla[19], and M. André[8]

[1]Department of Astrophysical and Planetary Sciences, University of Colorado Boulder, Boulder, Colorado, USA, [2]Laboratory of Atmospheric and Space Sciences, University of Colorado Boulder, Boulder, Colorado, USA, [3]Department of Physics, University of Colorado Boulder, Boulder, Colorado, USA, [4]The Blackett Laboratory, Imperial College London, London, UK, [5]Physics Department, University of New Hampshire, Durham, New Hampshire, USA, [6]Southwest Research Institute, San Antonio, Texas, USA, [7]Royal Institute of Technology, Stockholm, Sweden, [8]Swedish Institute of Space Physics, Uppsala, Sweden, [9]Department of Earth and Space Sciences, University of California, Los Angeles, California, USA, [10]NASA Goddard Space Flight Center, Greenbelt, Maryland, USA, [11]Department of Physics, University of Maryland, College Park, Maryland, USA, [12]Institut de Recherche en Astrophysique et Planétologie, Université de Toulouse, Toulouse, France, [13]Centre National de la Recherche Scientifique, Toulouse, France, [14]Laboratoire de Physique des Plasmas, Palaiseau, France, [15]Space Sciences Laboratory, University of California, Berkeley, California, USA, [16]Bartol Research Institute, Department of Physics and Astronomy, University of Delaware, Newark, Delaware, USA, [17]Department of Physics and Astronomy, West Virginia University, Morgantown, West Virginia, USA, [18]Space Research Institute, Austrian Academy of Sciences, Graz, Austria, [19]Department of Physics and Astronomy, University of California, Los Angeles, California, USA

Key Points:
- Magnetospheric Multiscale observations of large-amplitude, parallel, electrostatic waves associated with magnetic reconnection
- Simulations support that the strong electrostatic linear and nonlinear wave activities appear to be driven by a two-stream instability
- The frequent observation of these waves suggests that cold plasma is often present near the magnetopause

Correspondence to:
R. E. Ergun,
ree@lasp.colorado.edu

Citation:
Ergun, R. E., et al. (2016), Magnetospheric Multiscale observations of large-amplitude, parallel, electrostatic waves associated with magnetic reconnection at the magnetopause, *Geophys. Res. Lett.*, *43*, 5626–5634, doi:10.1002/2016GL068992.

Received 3 APR 2016
Accepted 10 MAY 2016
Accepted article online 13 MAY 2016
Published online 11 JUN 2016

Abstract We report observations from the Magnetospheric Multiscale satellites of large-amplitude, parallel, electrostatic waves associated with magnetic reconnection at the Earth's magnetopause. The observed waves have parallel electric fields ($E_{||}$) with amplitudes on the order of 100 mV/m and display nonlinear characteristics that suggest a possible net $E_{||}$. These waves are observed within the ion diffusion region and adjacent to (within several electron skin depths) the electron diffusion region. They are in or near the magnetosphere side current layer. Simulation results support that the strong electrostatic linear and nonlinear wave activities appear to be driven by a two stream instability, which is a consequence of mixing cold (<10 eV) plasma in the magnetosphere with warm (~100 eV) plasma from the magnetosheath on a freshly reconnected magnetic field line. The frequent observation of these waves suggests that cold plasma is often present near the magnetopause.

1. Introduction

Magnetic reconnection at the magnetopause occurs in an asymmetric setting between warm (~100 eV), dense (10 cm^{-3}–100 cm^{-3}) plasma in the magnetosheath and low-density (~1 cm^{-3}) plasma in the magnetosphere [e. g. *Paschmann et al.*, 2013, and references therein; *Hesse et al.*, 2014]. Both the magnetosheath plasma and magnetosphere plasma are highly variable in density (n) and electron and ion temperatures (T_e and T_i). The magnetosphere plasma contains hot (~1 keV) plasma but frequently has a cold (<10 eV) component as well.

Waves associated with magnetic reconnection at the magnetopause are well documented [e. g. *Labelle and Treumann*, 1988; *Deng and Matsumoto*, 2001; *Farrell et al.*, 2002; *Chaston et al.*, 2005; *Khotyaintsev et al.*, 2006]. The observation of whistler waves at the magnetopause, for example, has sparked debate on their role in magnetic reconnection [*Deng and Matsumoto*, 2001; *Vaivads et al.*, 2007; *Fujimoto and Sydora*, 2008]. The Magnetospheric Multiscale (MMS) mission [*Burch et al.*, 2016a] is designed to study magnetic reconnection at the magnetopause at high temporal and spatial resolution. This region also has been observed [*Paschmann et al.*, 2013] and studied with numerical simulations and analytic analysis [e. g. *Burch and Drake*, 2009, and references therein].

In this article, we present observations of intense, electrostatic waves that are parallel to the background magnetic field (***B***). The MMS mission provides unambiguous identification of the ion diffusion regions and electron

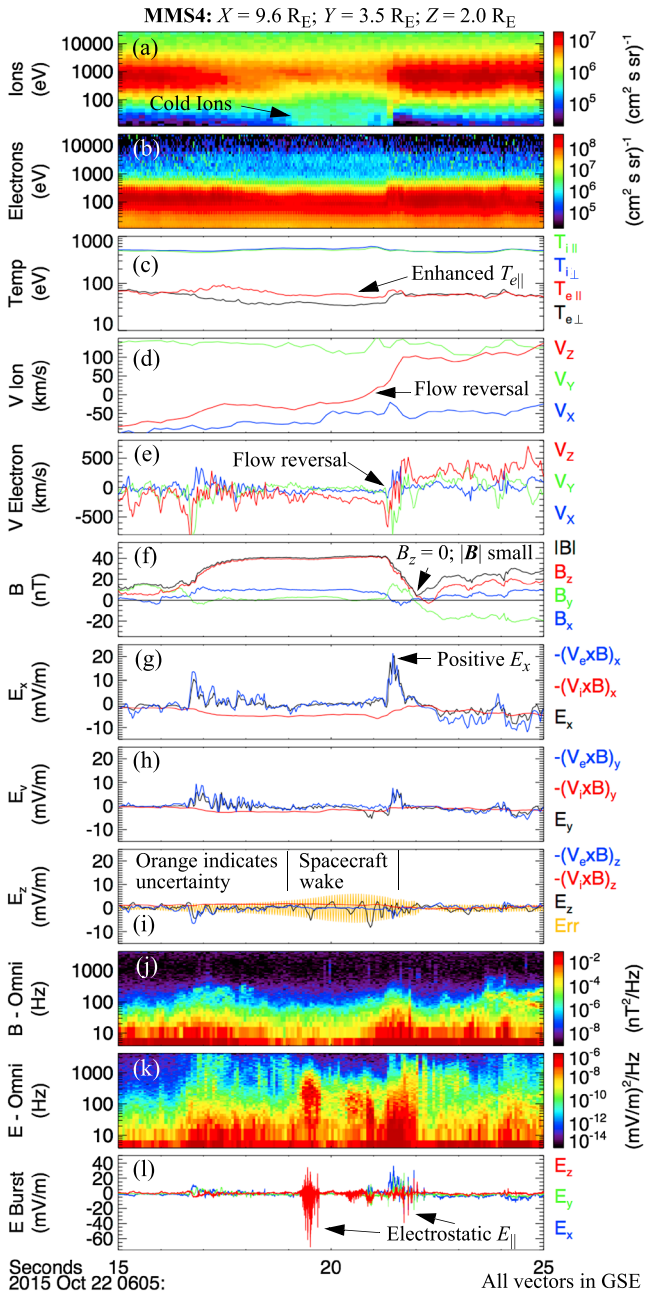

Figure 1. MMS4 observations on 22 October 2015 of a magnetic reconnection region. (a and b) The differential ion energy flux and differential electron energy flux as a function of energy (vertical axis) and time. (c) The parallel and perpendicular components of T_i and T_e. (d) $\boldsymbol{V}_i$. (e) $\boldsymbol{V}_e$. (f) $\boldsymbol{B}$. The black trace is $|\boldsymbol{B}|$. (g–i) $\boldsymbol{E}$ measured (black), $-\boldsymbol{V}_i \times \boldsymbol{B}$ (red), $-\boldsymbol{V}_e \times \boldsymbol{B}$ (blue). (j) The electric field spectral power density summed over all three components as a function of frequency (vertical axis) and time. (k) $\boldsymbol{E}$ in the frequency band of DC to ~3.2 kHz displayed at 8192 samples per second. All vectors are in GSE coordinates.

diffusion regions, allowing for detailed analysis of the relationship between waves and magnetic reconnection. We find that near (within several electron skin depths, λ_e) the electron diffusion region, large-amplitude (~25 mV/m to >200 mV/m), parallel electrostatic waves are frequently observed. In many of the observed cases, there is evidence of cold plasma.

To investigate the origin of these waves, we employ a 2-D Vlasov code [*Newman et al.*, 2001] to simulate the mixing of the warm magnetosheath plasma with a cold component in the magnetosphere. The results have good qualitative and quantitative agreement with observations. The waves appear to be driven by a two-stream instability (electron and/or ion) that results from plasma mixing. Several different wave modes can appear depending on the relative densities, temperatures, and drift speeds of the mixing plasmas. The strongest waves can be explained as electron acoustic waves [*Watanabe and Taniuti*, 1977; *Gary*, 1987] in regions where magnetosheath plasma is starting to penetrate into the magnetosphere. A beam mode appears if the cold plasma is accelerated into the magnetosheath plasmas. Ion acoustic waves also can be driven under specific density and temperature ratios. The wave modes can be a hybrid in that both the ion response of the magnetosheath plasma (traditional ion acoustic wave) and the electron response of the cold plasma (electron acoustic wave) can play a role. Because these waves are often within a few λ_e of the electron diffusion region, they may be a good indicator or marker of magnetic reconnection. The frequent occurrence of such waves, when near a magnetic reconnection site, supports previous findings that cold plasma is often present at the subsolar magnetopause [*Su et al.*, 2000; *McFadden et al.*, 2008; *Toledo-Redondo et al.*, 2015].

The intense, electrostatic waves are often observed in a nonlinear state with a possible net parallel potential. The 2-D Vlasov simulation results indicate that a parallel potential acts to retard magnetosheath electrons from an in-rush into the magnetosphere, preserving the quasi-neutral plasma. Such parallel electric fields

have been reported from laboratory experiments [e. g. *Carr et al*., 2013] and from several simulations of magnetic reconnections [*Li et al*., 2012; *Egedal et al*., 2015], albeit these simulations did not include a cold population. The same electric fields appear to accelerate cold electrons from the magnetosphere toward the reconnection site.

The large-amplitude, parallel, electrostatic waves are rarely observed in isolation. Often, observations over an extended region near the magnetic reconnection site include a mixture of waves including electrostatic whistler waves, lower hybrid waves, ion cyclotron waves, electromagnetic whistler waves, and Langmuir waves. The amplitudes and occurrence of the various wave modes are highly variable and are the subjects of future articles.

2. Observations

The observations in Figure 1 display 10 s of data (horizontal axis) from the MMS4 spacecraft near an electron diffusion region [*Burch and Drake*, 2009; *Burch et al*., 2016a, 2016b]. Figures 1a and 1b plot the ion and electron differential energy fluxes (color) as a function of energy (vertical axis) and time [*Pollock et al*., 2016]. Figure 1c plots the parallel and perpendicular measurements of T_i and T_e. The colors distinguish the measurements as labeled on the right side of the plot. Figures 1d and 1e plot the ion velocity ($\boldsymbol{V}_i$, 8 samples per second) and electron velocity ($\boldsymbol{V}_e$, 32 samples per second). Figure 1f plots $\boldsymbol{B}$ [*Torbert et al*., 2016; *Russell et al*., 2016] at 128 samples per second. All vector quantities and the spacecraft position at the top of the plot are in geocentric solar ecliptic (GSE) coordinates.

Figures 1g–1i display the three components of the electric field, E_x, E_y, and E_z, respectively [*Torbert et al*., 2016; *Lindqvist et al*., 2016; *Ergun et al*., 2016]. The measured electric field ($\boldsymbol{E}$) is in black, $-\boldsymbol{V}_e\times\boldsymbol{B}$ is in blue, and $-\boldsymbol{V}_i\times\boldsymbol{B}$ is in red. During this period, the uncertainty in the E_x and E_y components is ~1 mV/m. The uncertainty in the E_z component, however, varies. It increases to ~5 mV/m between ~06:05:19 UT and ~06:05:22 UT due a spacecraft wake, possibly from cold plasma [*Engwall et al*., 2006]. The uncertainty in E_z, is plotted in orange in Figure 1i, is derived from several sources including known measurement errors and offsets, and the time average of $\boldsymbol{E}\cdot\boldsymbol{B}$:

$$\Delta\boldsymbol{E} = \frac{1}{\Delta t}\int_{-\Delta t/2}^{\Delta t/2} \frac{\boldsymbol{E}\cdot\boldsymbol{B}\,\boldsymbol{B}}{|\boldsymbol{B}|^2}\,dt \tag{1}$$

$\Delta\boldsymbol{E}$ is derived from the $\boldsymbol{E}\cdot\boldsymbol{B}$ offset over an array of values of Δt starting at several hours reducing by a factor of 2 until Δt~10 s. The dominant contribution in the uncertainty (Figure 1i) comes with Δt~10 s. When large $\boldsymbol{E}\cdot\boldsymbol{B}$ offsets on time scales >10 s are seen, offset removal is implemented down to $\Delta t = 0.5$ s using medians rather than averages to preserve $E_{||}$ measurements of less than 0.5 s duration. An increase in uncertainty in the axial component suggests a possible cold plasma wake [*Engwall et al*., 2006]. The axial electric field measurement is most susceptible to spacecraft wake errors [e.g., *Cully et al*., 2007]. At the same time, the E_z uncertainty increases, a cold plasma component is observed in the ions (Figure 1a).

The data in Figure 1 suggest that the MMS4 spacecraft is near (within several λ_e) an electron diffusion region at 22 October 2015, ~06:05:22 UT (this event is briefly discussed by *Burch et al*. [2016b]). The indicators include a reversal in B_z and a near null in $|\boldsymbol{B}|$ (Figure 1f), increased parallel T_e (Figure 1c), a reversal in the Z component of $\boldsymbol{V}_i$ (Figure 1d), a reversal in the Z component of $\boldsymbol{V}_e$ (Figure 1e), and a positive E_x (Figure 1g) [e. g. *Shay et al*., 1998; *Hesse et al*., 2011; *Paschmann et al*., 2013, and references therein; *Shuster et al*., 2015]. In addition, Figures g–1i show good agreement between measured $\boldsymbol{E}$ and $-\boldsymbol{V}_e\times\boldsymbol{B}$, but $-\boldsymbol{V}_i\times\boldsymbol{B}$ noticeably differs, which indicates that the ions are de-coupled from the electrons and that MMS4 is in the ion diffusion region or a Hall electric field region, and near to the electron diffusion region.

Just before the magnetic reconnection event, the ions (Figure 1a) show the presence of ~10 eV plasma between ~06:05:19 UT and ~06:05:22 UT. At ~06:05:21.5 UT, perpendicularly convected cold ions are briefly observed at energies near ~20 eV to ~50 eV (see later, Figure 2a); after which, the cold ions are not observed. The convection of the cold ions appears to increase as the magnetic field decreases. An enhancement in the ~10 eV electrons is not clearly seen (Figure 1b); however, the ~10 eV electrons become field aligned (not displayed) between ~06:05:19 UT and ~06:05:22 UT. These observations and the possible detection of a spacecraft wake (Figure 1i) suggest that cold (<10 eV) plasma is present on the magnetosphere side from

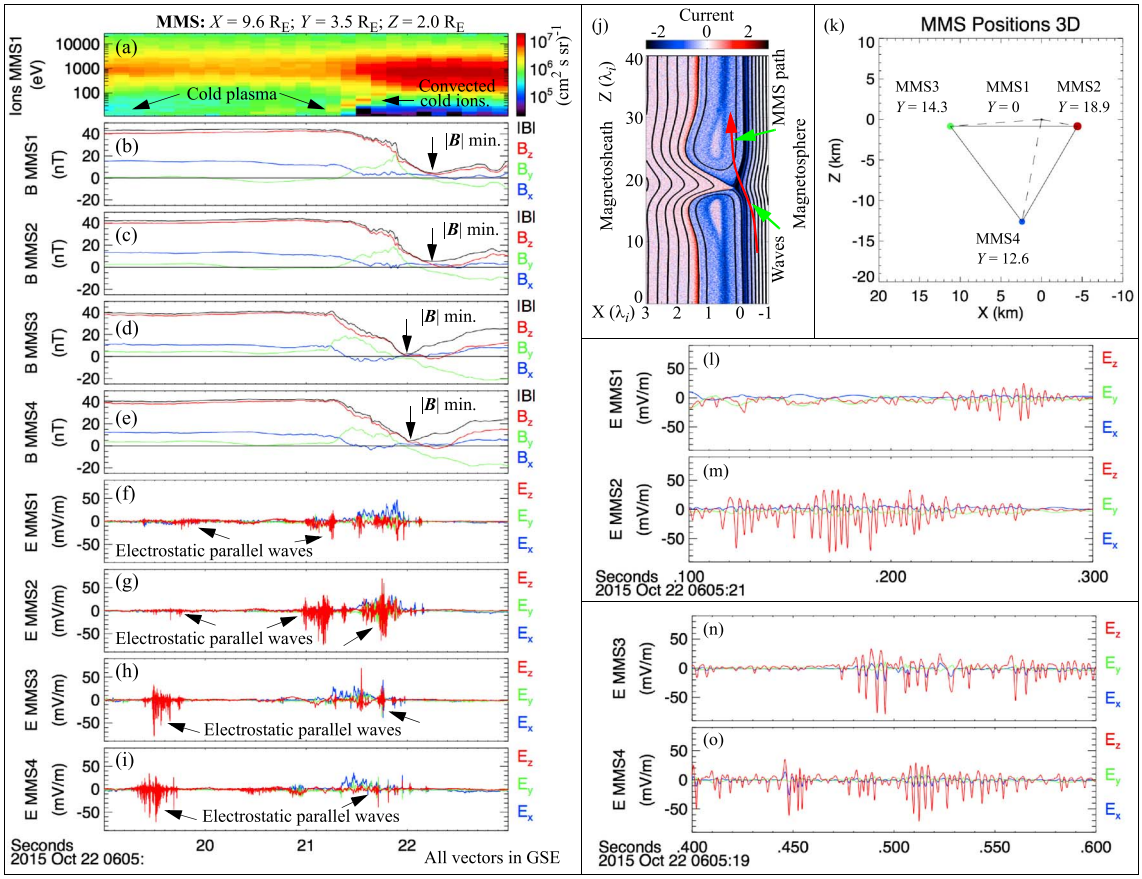

Figure 2. Observations of the event in Figure 1 from four MMS spacecraft. (a) The differential ion energy flux. (b–e) ***B***. (f–i) ***E***. (j) The approximate position of the MMS spacecraft (red line) inferred from observations plotted over a simulation of the magnetic reconnection region in the magnetopause [see *Lapenta et al.*, 2015]. $\lambda_i \sim 60$ km. (k) The relative positions of the MMS spacecraft in GSE coordinates. (l–o) Expanded views of wave emissions from Figures 2f–2i.

~06:05:19 UT to ~06:05:22 UT. Such cold plasma is supported by previous observations [*Su et al.*, 2000; *McFadden et al.*, 2008; *Toledo-Redondo et al.*, 2015].

At the same period that cold plasma is inferred, large-amplitude waves are observed (Figures 1j–1l). The red traces (which are nearly parallel to ***B***) just after ~06:05:19 UT (Figure 1l) are ~300 Hz waves as are the spiky red traces just before ~06:05:23 UT. The blue trace just after ~06:05:22 UT is dominated by a DC Hall electric field (see Figure 1g), so the waves are primarily parallel to ***B***. Figure 1j displays the omni-directional spectral power density of ***B*** [*Le Contel et al.*, 2016], and Figure 1k displays the omni-directional spectral power density of ***E***. Increased power in ***E*** is seen from ~50 Hz to ~1 kHz in frequency at the same time as the fluctuations in the red traces (Figure 1l). On the other hand, little or no enhancement is detected in ***B*** in the ~50 Hz to ~1 kHz frequency range, which indicates that the waves are electrostatic.

B, $\boldsymbol{V}_i$, and $\boldsymbol{V}_e$ observations (Figures 1d–1f) are consistent with the MMS position being near a magnetic reconnection region as displayed in Figure 2j. Prior to the reconnection event (~06:05:22 UT), B_z is positive and the Z components of $\boldsymbol{V}_i$ and $\boldsymbol{V}_e$ are negative, indicating that MMS is on the $-Z$ and $-X$ side of the reconnection region. After the reconnection event, B_z and $|\boldsymbol{B}|$ remain low. The ion distributions are typical of the magnetosheath, the B_y component begins to dominate, and $\boldsymbol{V}_i$ and $\boldsymbol{V}_e$ are positive.

Figure 2 displays the same event from all four MMS spacecraft. The time period is reduced to 4 s to highlight the region of the intense wave emissions. Figure 2a is the differential ion energy flux from MMS1 plotted in the same fashion as in Figure 1. Figures 2b–2e display ***B*** from the four MMS spacecraft at 128 samples per second. Figures 2f–2i display ***E*** (DC to ~3.2 kHz) at 8192 samples per second from the four MMS spacecraft in the same order. The relative positions of the four MMS spacecraft, which form a tetrahedron with separations of roughly 20 km, are displayed in Figure 2k.

The ion distributions show only small differences as seen by comparing Figures 1a and 2a. All of the MMS spacecraft infer a cold plasma prior to the magnetic reconnection event at ~06:05:22 UT. The magnetic fields display similar signatures. The minimum in $|\boldsymbol{B}|$ appears first in the MMS3 and MMS4 measurements (Figures 2d and 2e) and later in MMS1 and MMS2 observations (Figures 2d and 2e). The time delay is roughly 0.3 s. $\boldsymbol{E}$ observations on all four spacecraft show large-amplitude, electrostatic waves parallel to $\boldsymbol{B}$. These waves appear at different times indicating that the wave emissions are not coherent over a 20 km separation but can extend over regions greater than ~20 km.

Figures 2l and 2m display expanded views of the $\boldsymbol{E}$ waveforms (0.4 s time scales) from MMS1 and MMS2 about 1 s prior the $|\boldsymbol{B}|$ minimum. The waves are in the E_z direction, have frequencies between 100 Hz and 1 kHz, and display nonlinear evolution. The negative excursions are greater than the positive excursions, which would imply a net potential that retards electron flow from the magnetosheath into the magnetosphere. Figures 2n and 2o show expanded views of $\boldsymbol{E}$ waveforms (again, 0.4 s time scales) from MMS3 and MMS4 about 3.5 s prior the $|\boldsymbol{B}|$ minimum. The wave signatures have the same properties. Although no formal statistical study has been made, many dozens of similar events have been identified indicating that such emissions are frequent on the magnetosphereside of potential reconnection regions. Amplitudes often reach over 100 mV/m.

The wave powers in all of the events (Figures 2l–2o) are enhanced between ~100 Hz and ~1 kHz. The density (n) at that time is ~15 cm^{-3}. Accordingly, the ion plasma frequency (ω_{pi}) is ~800 Hz and the electron plasma frequency (ω_{pe}) is ~34 kHz. It is possible that the observed waves are ion acoustic, electron acoustic, or a beam mode. The wave power above ω_{pi} could be from Doppler shift. On the other hand, there are several similar observations at other times (not shown), in which the wave frequencies are considerably higher than ω_{pi} (almost all observations are show frequencies lower than ω_{pe}) suggesting electron acoustic waves.

3. Simulations

Prior observations of plasma waves at the magnetopause [e. g. *Labelle and Treumann*, 1988] include whistler waves [*Deng and Matsumoto*, 2001], Langmuir waves [*Farrell et al*., 2002], Alfvén waves [*Chaston et al*., 2005], and waves associated with turbulence [e. g. *Khotyaintsev et al*., 2006]. The MMS observations place intense parallel electrostatic wave activity within the ion diffusion region and adjacent (within a few λ_e) to the electron diffusion region. The data suggest that these waves may be ion acoustic, electron acoustic, or two-stream modes that are driven from the mixing of the warm, O(100 eV), dense, O(10 cm^{-3}), magnetosheath plasma with cold ($<$10 eV), low-density ($<$1 cm^{-3}) plasma in the magnetosphere. The basic idea is that on a freshly reconnected plasma line, warm, dense magnetosheath electrons are expected to flow into the magnetosphere. This electron inrush can drive a two-stream instability resulting in ion acoustic, electron acoustic, or beam mode emissions. The magnetosheath ions move at slower speeds, so a retarding electric field is expected to develop to slow the electron inrush. This same retarding electric field can accelerate the cold plasma in the magnetosphere into beam, which, again, can drive strong waves. The wave modes depend on the densities and temperatures of the magnetosheath plasma and those of the cold plasma in the magnetosphere. The hot (~1 keV) population in the magnetosphere is unlikely to play a strong role.

To explore the generation of these waves, we perform a basic Vlasov simulation in two spatial dimensions [*Newman et al*., 2001] of plasma mixing at the magnetopause. The simulation covers 2400×300 Debye lengths (λ_D) in the spatial domain corresponding to roughly 48×0.6 km. The simulation extends ± 6 v_{thew} (v_{thew} is the thermal velocity of the warm magnetosheath population) in the velocity domain. The mass ratios are realistic. The simulation is strongly magnetized in one spatial direction (Z) but allows for development of oblique modes (see *Newman et al*. [2001] for details). The parallel direction (Z direction) has open boundaries. The perpendicular boundaries are periodic.

Figure 3a displays a snapshot of the electron distribution early in the simulation. The simulation was initialized with representative magnetosheath ion and electron distributions ($n = 30$ cm^{-3}; T_e, $T_i = 100$ eV) on the right side and cold plasma ($n = 2$ cm^{-3}; T_e, $T_i = 1$ eV) on the left side. The boundary between the two plasmas was smoothed over 120 λ_D to prevent a large transient upon startup.

Almost immediately after start, the magnetosheath electrons flow into the magnetosphere and a parallel electric field develops to retard the electron inrush. The parallel electric field accelerates the cold magnetosphere

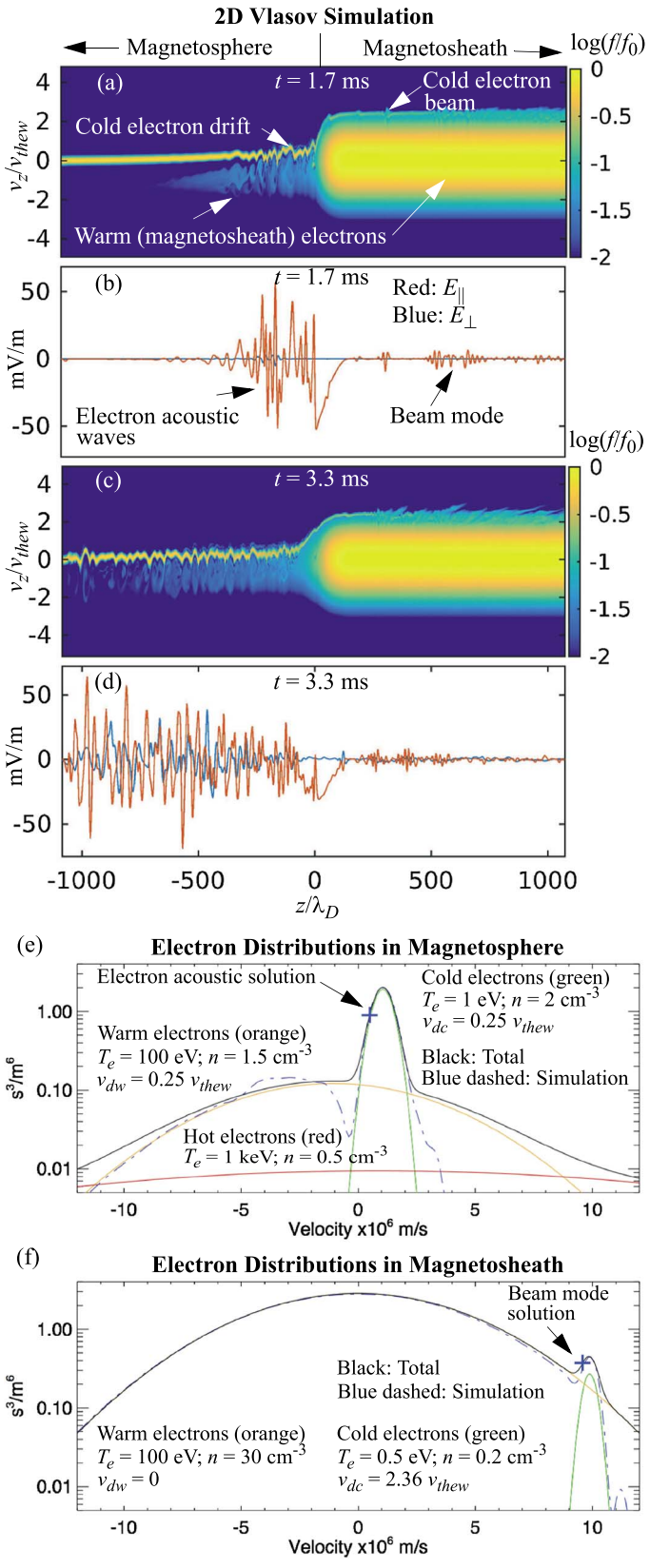

electrons into a beam directed toward the magnetosheath. Strong parallel waves are seen on both sides of the boundary (Figure 3b). The largest amplitude waves are on the magnetosphere side, which appear to be primarily electron acoustic driven by the relative streaming of the two electron populations. The magnetosheath electrons are streaming to the left with respect to the cold electrons, which, in turn, are drifting toward the magnetosheath. The parallel waves on the right side appear to come from a much higher velocity two-stream or beam instability driven by accelerated cold electrons (Figure 3a).

In the simulation frame, the waves on the left side have a frequency

Figure 3. A Vlasov simulation of the cold (1 eV) magnetosphere plasma mixing with warm magnetosheath plasma (100 eV). (a) The electron distribution early in the simulation. The dense (30 cm^{-3}) magnetosheath electrons flow into the magnetosphere (2 cm^{-3}) setting up a retarding electric field, which, in turn, accelerates the cold electrons into the magnetosheath. (b) Initially, electron acoustic modes develop on the magnetosphereside while a beam mode appears on the magnetosphere side. (c) Later in the simulation, the magnetosheath electrons (and ions, not shown) penetrate farther into the magnetosphere. (d) Oblique modes develop at later times. (e) A model of the electron distribution on the magnetosphereside showing the electron acoustic mode solution with a frequency of ~300 Hz in the plasma rest frame. The hot electrons are included then removed to demonstrate that the hot population does not significantly influence wave growth. The blue dashed line is an electron distribution from the simulation, compiled from several distributions from $z/\lambda_D = -250$ to $z/\lambda_D = -80$. (f) A model of the electron distributions on the magnetosheath side showing the beam mode solution. Again, the frequency is ~300 Hz in the plasma rest frame. The blue dashed line is an electron distribution from the simulation at $z/\lambda_D = 200$.

of ~600 Hz. However, since the wavelengths (25 λ_D, λ_D~12 m) are on the order of 300 m, a change in drift velocity of the electrons, a change in the plasma properties, or a Doppler shift could result in a significant difference in an observed frequency. The frequency the observed waves (~300 Hz) compares well, given the uncertainties. The waves on the right side of the simulation have significantly higher frequency, on the order of 10–20 kHz, which is below the local plasma frequency. Again, these waves can have significantly different frequencies in observations due to a change in the cold plasma drift velocity or a Doppler shift.

An analytic analysis is used to identify the wave modes. The dispersion relation

$$\epsilon = 1 + \chi_e^c + \chi_e^w + \chi_e^h + \chi_i^c + \chi_i^w + \chi_i^h \tag{2}$$

can be solved numerically from the Fried-Conte dispersion relation [*Fried and Conte*, 1961]. Here $\chi_e{}^c$ represents the parallel susceptibility of cold magnetosphere electrons, $\chi_e{}^w$ represents warm magnetosheath electrons, and $\chi_e{}^h$ represents hot electrons, often seen in the magnetosphere. The subscript (*i*) represents the ion susceptibilities. In almost all cases that we explore $\chi_e{}^h$ and $\chi_i{}^h$ can be ignored. In general, there can be multiple roots to equation (2). The solutions are not necessarily well-established normal modes often derived in Maxwellian plasmas.

Figure 3e displays modeled electron distributions on the magnetosphere side (left side) of the simulation. The electron instrument on MMS [*Pollock et al*., 2016] does not resolve electrons below ~10 eV, so a direct comparison of measured electron distributions with those in the simulation is not possible. An electron distribution from the simulation, compiled from several distributions from $z/\lambda_D = -250$ to $z/\lambda_D = -80$, is plotted as a dashed blue line. The hot electrons from the simulation have strong variation as a function of velocity due to the strong nonlinear wave activity. The modeled electrons and ions are represented as a set of drifting Maxwellian distributions to best reproduce the electrons observed in the simulation. Equation (2) is used to solve for roots (wave modes) and growth. The cold electrons are modeled as a drifting (positive is toward the right or magnetosheath) 1 eV population with a density of 2 cm^{-3}. The warm electrons that have penetrated into the magnetosphere are assigned a density of 1.5 cm^{-3} and are flowing into the magnetosphere as seen in Figure 3a. The electron densities, temperatures, and drift speeds are on the Figure 3e. A hot population of 0.5 cm^{-3} with $T_e = 1$ keV was added and then removed to verify that the hot population does not noticeably influence the results.

The waves on the magnetosphere side are best described as electron acoustic waves with $\chi_e{}^w \sim \omega_{pew}{}^2/(\gamma k_{||} v_{thew})^2$ (acoustic response) offsetting $\chi_e{}^c \sim -\omega_{pec}{}^2/(\omega - k_{||} v_{dc})^2$ (Doppler shifted plasma response). Here ω_{pec} and ω_{pew} are electron plasma frequencies of the cold and warm electrons, ω is the wave frequency, $k_{||}$ is the wave vector, v_{thew} is the thermal velocity of the warm electrons, and v_{dc} is the drift velocity of the cold electrons with respect to the center of mass of all electrons. The electron acoustic wave mode shows positive growth under a variety of densities and temperatures as long as $v_{thec} < v_{dc} < v_{thew}$, where v_{thec} is the thermal velocity of the cold electrons.

Figure 3f displays the modeled electron distributions on the magnetosheath side (right side) of the simulation. The blue dashed line represents an electron distribution from the simulation at $z/\lambda_D = 200$. The cold electrons are drifting into nearly stationary warm electrons at ~2.4 v_{thew}. In this case, $\chi_e{}^w \sim -\omega_{pew}{}^2/\omega^2$ (plasma response) is offset by $\chi_e{}^c$ with a positive acoustic-like response. $\chi_e{}^c$ is difficult to describe analytically as it has a strong imaginary contribution. This mode is best described as a beam mode as $v_{dc} > v_{thew}$. Notably, the ion susceptibilities can participate or even dominate if the drift speeds, densities, or temperatures are such that the electron acoustic mode or beam mode cannot develop. Under these conditions, the ion acoustic modes dominate. We cannot rule out the possibility that the observed waves (Figure 1) are ion acoustic without detailed observations of the cold ion and cold electron distributions.

The simulation results (Figures 3a and 3b) suggest that parallel wave modes dominate the initial stage of mixing of the cold magnetosphere plasma and magnetosheath plasma. The two-stream instability appears to have the fastest growth rate. The initial mixing is expected to be near the electron diffusion region. As a result, the simulation results support that parallel waves are observed near the electron diffusion region.

Figure 3c displays the electron distribution at a later time (3.3 ms, ~1000 time steps of $1/\omega_{pew}$) in the simulation. The magnetosheath electrons (and ions, not shown) have penetrated farther into the magnetosphere. The retarding electric field is decreased but extended. Large-amplitude parallel waves remain, but oblique waves begin to appear (Figure 3d).

Interestingly, the beam mode and electron acoustic roots, the real part of equation (2), can vanish as distributions are altered by quasi-linear and nonlinear diffusion before the distributions are stabilized. It is possible that at a later time and thus at larger distances from the electron diffusion region (or mixing region), oblique modes such as whistler waves, lower hybrid waves, and ion cyclotron waves can develop. Observation of oblique modes on reconnected field lines farther from the mixing region is in concert with prior observations [e.g., *Labelle and Treumann*, 1988]. Oblique waves are also observed by MMS (not shown) farther from the electron diffusion region. The simulation, however, could not be run on a large enough domain or for a long enough time to determine if oblique modes dominate far from the mixing region.

4. Discussion and Conclusions

MMS observations allow us to accurately place magnetopause wave modes in context of the ion diffusion region and electron diffusion region. Wave activity at the magnetopause otherwise has been well documented [e. g. *Labelle and Treumann*, 1988]. MMS observations, supported by simulations, suggest that the large-amplitude, parallel, electrostatic waves are driven by a two-stream instability due to plasma mixing on a newly reconnected magnetic field. MMS observes these waves frequently inside of the ion diffusion region and adjacent to the electron diffusion region. The Vlasov simulations suggest that parallel, electrostatic waves dominate in early evolution of the mixing process. These results suggest that large-amplitude, parallel, electrostatic waves are a good indication of a nearby electron diffusion region. The frequent observation of such waves also suggests that cold plasma is common at regions of magnetic reconnection.

It is unclear if the parallel waves could have a direct influence on the magnetic reconnection process. It is significant that the observed waves have evolved to a nonlinear state that has a possible net parallel potential. The direction of a net potential is such that it would act to retard electrons moving from the magnetosheath into the magnetosphere. Such electric fields in the form of double layers have been reported in simulations relevant to solar magnetic reconnection [*Li et al*., 2012; *Egedal et al*., 2015]. Such a potential can alter the electron and ion distributions in the electron diffusion region and, possibly affect the reconnection process.

Acknowledgments
This work was funded by the NASA MMS project. The authors recognize the tremendous effort in developing and operating the MMS spacecraft and instruments and sincerely thank all involved. MMS data are open to the public. The IRAP contribution to MMS was supported by CNES.

References

Burch, J. L., and J. F. Drake (2009), Reconnecting magnetic fields, *Am. Sci.*, *97*, 392–399.
Burch, J. L., T. E. Moore, R. B. Torbert, and B. L. Giles (2016a), Magnetospheric Multiscale overview and science objectives, *Space Sci. Rev.*, *199*, 5–21, doi:10.1007/s11214-015-0164-9.
Burch, J. L., et al. (2016b), Electron-scale measurements of magnetic reconnection in space, *Science*, doi:10.1126/science.aaf2939, in press.
Carr, J., Jr., et al. (2013), Spontaneous ion beam formation in the laboratory, space, and simulation, *Phys. Plasmas*, *20*, 072118, doi:10.1063/1.4817263.
Chaston, C. C., et al. (2005), Drift-kinetic Alfvén waves observed near are connection X line in the Earth's magnetopause, *Phys. Rev. Lett.*, *95*, 065002, doi:10.1103/PhysRevLett.95.065002.
Cully, C. M., R. E. Ergun, and A. I. Eriksson (2007), Electrostatic structure around spacecraft in tenuous plasma, *J. Geophys. Res.*, *112*, A09211, doi:10.1029/2007JA012269.
Deng, X. H., and H. Matsumoto (2001), Rapid magnetic reconnection in the Earth's magnetosphere mediated by whistler waves, *Nature*, *410*, 557–560, doi:10.1038/35069018.
Egedal, J., W. Daughton, A. Le, and A. L. Borg (2015), Double layer electric fields aiding the production of energetic flat-top distributions and superthermal electrons within the exhausts from magnetic reconnection, *Phys. Plasmas*, *22*(10), 101208.
Engwall, E., A. I. Eriksson, M. André, I. Dandouras, G. Paschmann, J. Quinn, and K. Torkar (2006), Low-energy (order 10 eV) ion flow in the magnetotail lobes inferred from spacecraft wake observations, *Geophys. Res. Lett.*, *33*, L06110, doi:10.1029/2005GL025179.
Ergun, R. E., et al. (2016), The axial double probe and fields signal processing for the MMS mission, *Space Sci. Rev.*, *199*, 67–188, doi:10.1007/s11214-014-0115-x.
Farrell, W. M., M. D. Desch, M. L. Kaiser, and K. Goetz (2002), The dominance of electron plasma waves near a reconnection X-line region, *Geophys. Res. Lett.*, *29*(19), 1902, doi:10.1029/2002GL014662.
Fried, B. D., and S. D. Conte (1961), *The Plasma Dispersion Function*, Academic Press, San Diego, Calif.
Fujimoto, K., and R. D. Sydora (2008), Whistler waves associated with magnetic reconnection, *Geophys. Res. Lett.*, *35*, L19112, doi:10.1029/2008GL035201.
Gary, S. P. (1987), The electron/electron acoustic instability, *Phys. Fluids*, *30*(9), 2745–2749, doi:10.1063/1.866040.
Hesse, M., T. Neukirch, K. Schindler, M. Kuznetsova, and S. Zenitani (2011), The diffusion region in collisionless magnetic reconnection, *Space Sci. Rev.*, *160*, 3–23, doi:10.1007/s11214-010-9740-1.
Hesse, M., N. Aunai, D. Sibeck, and J. Birn (2014), On the electron diffusion region in planar, asymmetric, systems, *Geophys. Res. Lett.*, *41*, 8673–8680, doi:10.1002/2014GL061586.
Khotyaintsev, Y. V., A. Vaivads, A. Retinò, M. André, C. J. Owen, and H. Nilsson (2006), Formation of inner structure of a reconnection separatrix region, *Phys. Rev. Lett.*, *97*(20), 205003, doi:10.1103/PhysRevLett.97.205003.
Labelle, J., and R. A. Treumann (1988), Plasma waves at the dayside magnetopause, *Space Sci. Rev.*, *47*, 175–202, doi:10.1007/BF00223240.
Lapenta, G., S. Markidis, M. V. Goldman, and D. L. Newman (2015), Secondary reconnection sites in reconnection-generated flux ropes and reconnection fronts, *Nat. Phys.*, *11*, 690–695, doi:10.1038/nphys3406.
Le Contel, O., et al. (2016), The search-coil magnetometer for MMS, *Space Sci. Rev.*, *199*, 257–282, doi:10.1007/s11214-014-0096-9.

Li, T. C., J. F. Drake, and M. Swisdak (2012), Supression of energetic electron transport in flares by double layers, *Astrophys. J.*, *757*, doi:10.1088/0004-637X/757/1/20.

Lindqvist, P.-A., et al. (2016), The spin-plane double probe instrument for MMS, *Space Sci. Rev.*, *199*, 137–165, doi:10.1007/s11214-014-0116-9.

McFadden, J., C. Carlson, D. Larson, J. Bonnell, F. Mozer, V. Angelopoulos, K.-H. Glassmeier, and U. Auster (2008), Structure of plasmaspheric plumes and their participation in magnetopause reconnection: First results from THEMIS, *Geophys. Res. Lett.*, *35*, L17S10, doi:10.1029/2008GL033677.

Newman, D. L., M. V. Goldman, M. Spector, and F. Perez (2001), Dynamics and instability of electron phase-space tubes, *Phys. Rev. Lett.*, *86*, 1239–1242.

Paschmann, G., M. Øieroset, and T. Phan (2013), In-situ observations of reconnection in space, *Space Sci. Rev.*, *47*, 309–341, doi:10.1007/978-1-4899-7413-6_12.

Pollock, C., et al. (2016), Fast plasma investigation for Magnetospheric Multiscale, *Space Sci. Rev.*, *199*, 331–406, doi:10.1007/s11214-016-0245-4.

Russell, C. T., et al. (2016), The Magnetospheric Multiscale magnetometers, *Space Sci. Rev.*, *199*, 189–256, doi:10.1007/s11214-014-0057-3.

Shay, M. A., J. F. Drake, R. E. Denton, and D. Biskamp (1998), Structure of the dissipation region during collisionless magnetic reconnection, *J. Geophys. Res.*, *103*(A5), 9165–9176, doi:10.1029/97JA03528.

Shuster, J. R., L.-J. Chen, M. Hesse, M. R. Argall, W. Daughton, R. B. Torbert, and N. Bessho (2015), Spatiotemporal evolution of electron characteristics in the electron diffusion region of magnetic reconnection: Implications for acceleration and heating, *Geophys. Res. Lett.*, *42*, 2586–2593, doi:10.1002/2015GL063601.

Su, Y.-J., J. E. Borovsky, M. F. Thomsen, R. C. Elphic, and D. J. McComas (2000), Plasmaspheric material at the reconnecting magnetopause, *J. Geophys. Res.*, *105*, 7591–7600, doi:10.1029/1999JA000266.

Toledo-Redondo, S., A. Vaivads, M. André, and Y. V. Khotyaint- sev (2015), Modification of the hall physics in magnetic reconnection due to cold ions at the Earth's magnetopause, *Geophys. Res. Lett.*, *42*, 6146–6154, doi:10.1002/2015GL065129.

Torbert, R. B., et al. (2016), The FIELDS instrument suite on MMS: Scientific objectives, measurements, and data products, *Space Sci. Rev.*, *199*, 105–135, doi:10.1007/s11214-014-0109-8.

Vaivads, A., O. Santolík, G. Stenberg, M. André, C. J. Owen, P. Canu, and M. Dunlop (2007), Source of whistler emissions at the dayside magnetopause, *Geophys. Res. Lett.*, *34*, L09106, doi:10.1029/2006GL029195.

Watanabe, K., and T. Taniuti (1977), Electron-acoustic mode in a plasma of two-temperature electrons, *J. Phys. Soc. Jpn.*, *43*(5), 1819–1820, doi:10.1143/JPSJ.43.1819.